

Article

Characteristic Developments of the Water-Conducting Fracture Zones in Weakly Cemented Overlying Strata of Jurassic Coal Mines in Western China

Lifei Zhang ^{1,2} , Zizhao Zhang ^{1,3,*}, Kaikai Wang ¹ , Xiaodong Tan ¹, Tiandong Zhang ¹ and Lei Zhang ¹¹ School of Geology and Mining Engineering, Xinjiang University, Urumqi 830046, China² The First Regional Geological Survey Brigade, Xinjiang Bureau of Geo-Exploration & Mineral Development, 466 North Tianjin Road, Urumqi 830011, China³ State Key Laboratory for Geomechanics and Deep Underground Engineering, Xinjiang University, Urumqi 830046, China

* Correspondence: zhangzizhao@xju.edu.cn; Tel.: +86-136-3997-7295

Abstract: The overlying weakly cemented, and poorly performing strata in Jurassic mines of western China have mechanical properties that are generally lower than those in the Carboniferous-Permian coal mines of central and east China. During coal mining, the overlying strata easily deform and fracture. These then formed water-conducting channels, triggering a series of eco-environmental issues, including ground fracturing, collapsed surfaces, declined underground water levels, deserted lands, and even severe water/sand burst accidents. To study the fracture characteristics of weakly cemented overlying strata and the evolution law of water-conducting fractures in Jurassic coal mines in western China, this study selected Tashidian Erjingtian Mine in Korla, Xinjiang, as the research object. Based on the simulation data obtained with physical analog model testing and field monitoring results, the authors investigated the development of water-conducting fractures in the weakly cemented overlying strata during the coal seam mining process. We simultaneously determined the location of key strata in the working face based on key stratum theory. According to the present research results, key strata controlled the development height of water-conducting fractures. When the primary key stratum or sub-key stratum was not fractured, the development of water-conducting fractures was stagnant; water-conducting fractures developed abruptly when the primary key stratum or sub-key stratum was cracked. The heights of water-conducting fractures in the weakly cemented overlying strata of western China exceeded that of similar stopes of central and east China. These research results provided theoretical and technical support for safety in production at Tashidian Coal Mine. In addition, they offered a reference for green and safe production in Jurassic coal mines of western China.

Keywords: Jurassic coal mining area in western China; weakly cemented overlying strata; physical analog model; key stratum theory; the height of the water-conducting fracture zone



Citation: Zhang, L.; Zhang, Z.; Wang, K.; Tan, X.; Zhang, T.; Zhang, L. Characteristic Developments of the Water-Conducting Fracture Zones in Weakly Cemented Overlying Strata of Jurassic Coal Mines in Western China. *Water* **2023**, *15*, 1097. <https://doi.org/10.3390/w15061097>

Academic Editor: Lahcen Zouhri

Received: 11 October 2022

Revised: 13 February 2023

Accepted: 9 March 2023

Published: 13 March 2023



Copyright: © 2023 by the authors. Licensee MDPI, Basel, Switzerland. This article is an open access article distributed under the terms and conditions of the Creative Commons Attribution (CC BY) license (<https://creativecommons.org/licenses/by/4.0/>).

1. Introduction

Currently, coal resource development in east China has almost ended. The exploration of coal resources has started the strategic shift, i.e., the investigation has moved to the western regions that are more abundant in resource reserves. Jurassic coal-bearing strata in west China show short diagenetic periods that differ from the Carboniferous and Permian strata in central and east China. The overlying strata show weakly cemented argillaceous characteristics when encountering water, with low strength, poor cementing and easy-to-collapse performance, and a lower residual crack-expansion coefficient of rock [1–3]. Many researchers have studied rock–water interaction through various methods, and have explored soft rock softening and its mechanism [4–8]. Weakly cemented

rocks with weak performance contain many clay minerals, including montmorillonite, illite, and kaolinite [9]. Accordingly, weakly cemented rocks' internal friction angle and cohesive force are low. As a result, the overlying rocks showed low self-bearing capacity, poor self-stabilization capacity, and short self-stabilization time.

After the excavation of coal seams, a series of engineering disasters, including heavy deformation and roof caving, quickly appeared in the weakly cemented overlying rocks, seriously affecting mine construction, safety, and high-efficiency production. Weakly cemented rocks can be hard rocks in dry or natural conditions; however, when saturated, weakly cemented rocks fall between soft rock and hard soil in terms of physical and mechanical properties and are regarded as transitional rock media [10]. Researchers have conducted a great deal of research on the physical and mechanical properties of soft rock [11–15]. Atapour concluded that the mechanical properties of cemented materials mainly determine the mechanical characteristics of weakly cemented rocks [16]. Li et al. used experimental studies on microstructures and mechanical response characteristics of weakly cemented rocks with a scanning electron microscope and low-field nuclear magnetic resonance (NMR) [17,18]. According to previous research results, the content of weakly cemented sandstone is relatively low, with a low cementing degree, large porosity, and loose structure, leading to reasonably low compressive strength and elasticity modulus of weakly cemented sandstone and great deformation. During the excavation process, deformation-induced damage to the overlying strata quickly appeared in the weakly cemented strata. Then, water-conducting channels triggered a series of environmental problems and water/soil inrush accidents, mainly including the formation of ground fractures, surface collapse, the decline of underground water level, water and soil erosion, and water/sand inrush accidents. Coal mining imposes enormous effects on the utilization of water resources. Western China experiences severe scarcity of water resources and relatively vulnerable natural ecological conditions. Any carelessness in the extensive development and utilization of coal resources is highly likely to cause irreversible ecological damages [19]. Therefore, prevention and treatment of roof water disasters in Jurassic coal mines of western China and water resources preservation during mining have always been hot topics arousing extensive concern. In particular, predicting the development height of the water-conducting fractured zone was a crucial link [20,21].

Coal resources in China's weakly cemented strata are primarily in several main coal bases, including Xinjiang, Shandong, the northern region of Shanxi, the eastern province of Ningxia, the northern part of Shaanxi, Huanglong, the eastern part of Inner Mongolia, and the Yunnan-Guizhou region. The mines in western and northwestern China occupy the most significant proportion. Currently, Xinjiang coal bases are in the early-stage development phase, while other main coal bases are in the middle-term development phases. Fourteen coal base reserves accounted for 50.4% of China's coal reserves. Mining weakly cemented strata coal resource base reserves accounted for approximately 54.09%. Of the 14 base reserves, nearly half of the resources are in weakly cemented strata [22]. In the past, the research on the development height of the water-conducting fracture zone was primarily concentrated in the Carboniferous-Permian coal mining area in central and eastern China. There were few studies in the western mining area. Many researchers focused on the prediction of the development height of the water-conducting fracture zone [23–29] utilizing physical experiment, numerical simulation, theoretical analysis, geophysical exploration, underground segmented water injection, leakage observation of drilling fluid, and borehole TV. This study focused on Tashidian Mine, Korla City, Xinjiang, China. First, it investigated the development characteristics of water-conducting fractures in weakly cemented overlying strata during the coal seam mining process based on a physical model test on similar materials. Next, according to key stratum theory, this study determined the critical stratum position in the overlying strata of the working face. On that basis, we concluded the fracturing characteristics of overlying strata and the evolution rules of water-conducting fractures. The present research results can provide theoretical support

for safety production in Tashidian Coal and a reference for green and safety production in Jurassic coal mines of western China.

2. Project Profile

The research region, located in Korla City, Bayingol Mongolian Autonomous Prefecture, Xinjiang, belongs to southern Xinjiang (see Figure 1). Tashidian mine is located at the southwestern margin of Yanqi Basin and shows lower and middle hilly land. In terms of terrain, the western regions are higher, the middle is lower, the northern part is higher, and the southern part is even lower. This study focused on the W8203 working face owned by Tashidian Coal at the western edge of the well. In the primary mineable No. 8 coal seam, the length and the width of the working face are 1588 and 135 m, respectively, with a mean thickness of the coal seam of approximately 9.6 m. Mining was carried out with fully mechanized top coal caving and a controlled roof with caving. As a result, the roof and floor were easily inflated and softened when encountering water.

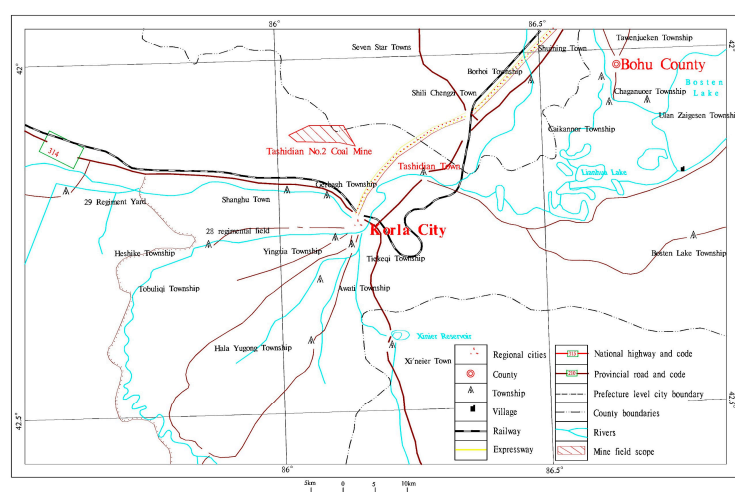


Figure 1. Illustration of the traffic position of the research area.

Mining seams are located at the weak-water-abundance aquifer (H_3) on the bearing fractures of the middle Jurassic Tashidian formation. As shown in Figure 2 (see Figure S1 in Supplementary Material), four aquifers and aquicludes were above the mining coal seam, which was the Quaternary permeable stratum. The aquiclude was of clayey mudstone and siltstone in the Putaogou formation of the Neogene Pliocene series. The weak-water-abundant aquifer on the bearing fractures of Oligocene-Miocene Taoshuyuan Formation in the Paleogene series and the aquiclude consist of paleo crust of weathering mudstone, siltstone, and fine sandstone.

Aquifer (H_1) is the main indirect water-filled aquifer in the coal mine. The pumping test of aquifer (H_1) was carried out in the North 10–5 hole and the North 12–6 hole with the nature of confined water. The thickness of the exposed strata was 9.74–138.04 m, with an average thickness of 97.45 m. The thickness of aquifer (H_1) is 106.99–138.04 m, the static water level elevation is 1103.59–1124.183 m, the water inflow is 0.12–1.046 L/s, and the permeability coefficient is 0.0097–0.0294 m/d. Aquifer (H_3) is the direct water-filled aquifer of No.8 coal seam. The pumping test was carried out in aquifer (H_3) in the North 10–5 hole and the North 12–6 hole with confined water properties. The drilling revealed that the thickness was 28.66–193.74 m, and the average thickness was 72.92 m. The static water level elevation is 1102.59–1124.083 m, the water inflow is 0.039–0.14 L/s, and the permeability coefficient is 0.0019–0.0065 m/d. According to the completed pumping test the inflow of water, static water level elevation, permeability coefficient and porosity of aquifer (H_1) and aquifer (H_3) are shown in Table 1. A map of the groundwater flow is shown in Figure 3.

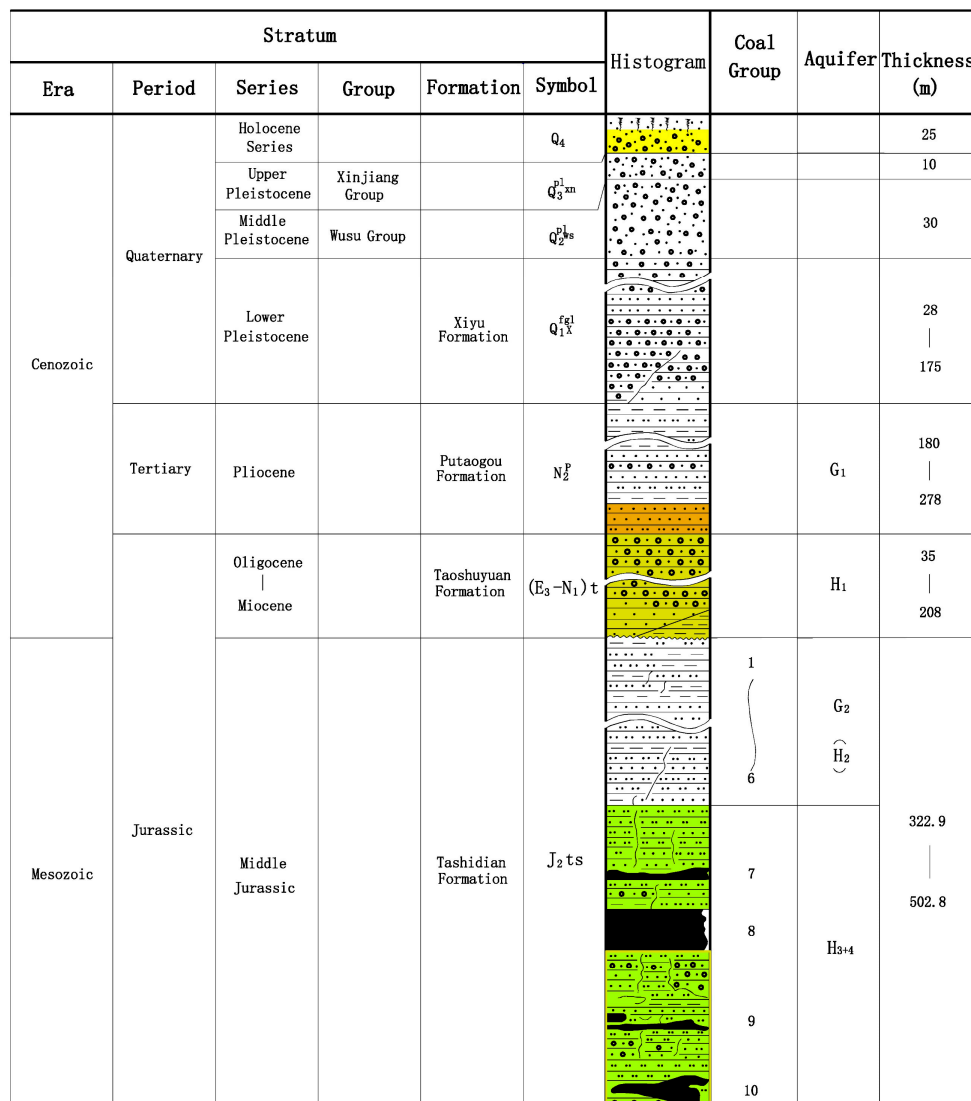


Figure 2. Synthetic hydrogeological histograms of Tashidian Erjingtian Mine.

Table 1. Aquifer pumping test results table.

Aquifer	Pumping Test Hole	Inflow of Water (L/s)	Static Water Level Elevation (m)	Permeability Coefficient (m/d)	Porosity (%)
H ₁	North 10–5	0.12–0.34	1124.183	0.0097–0.0104	3.45–6.99
	North 12–6	0.332–1.046	1103.59	0.0225–0.0294	3.45–6.99
H ₃	North 10–5	0.039	1124.083	0.0019	1.15–6.62
	North 12–6	0.14	1102.59	0.0065	1.15–6.62

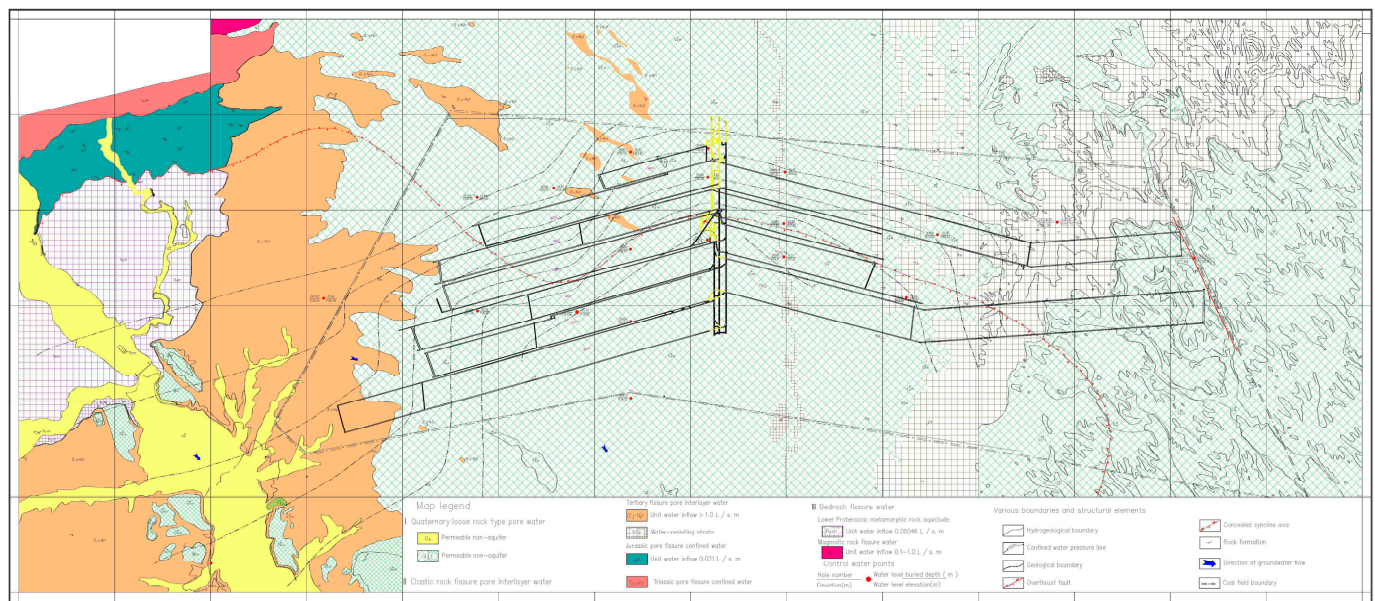


Figure 3. Map of the groundwater flow.

Under mining, the weak-water-abundant aquifer (H3) structure bearing on the fractures of the middle Jurassic Tashidian formation destroyed the height of the water-conducting fracture zone beyond the mining range, leading to the formation of water-conducting channels. The water-conducting channels were then interconnected to the upper aquifer/aquiclude, imposing certain damages to the aquifer structure. According to the statistics in recent years, the regular water inflow of the mine is approximately 3000 m³/d, with a maximum value of 5040 m³/d (in the goaf drainage period), and the loss of underground water resources is excellent. A few species feature in the plant community in the mine. However, the ecological environment was highly vulnerable, with a vegetation coverage rate of only 5%. Mining-induced underground resource loss further aggravated the deterioration of the ecological environment in the mine.

Based on the stratigraphic information of the mine and the related exploration data, the physical and mechanical parameters of the overlying strata were investigated and determined, as shown in Table 2. Through analysis, the strata were mainly in argillaceous cementation, with low overall strength. The uniaxial compressive strength of most strata is lower than 30 MPa. The overlying strata have a loose structure and show easy weathering. According to the related definitions in most studies, the overlying strata in the research mine was regarded as weakly cemented overlying strata [30].

Table 2. Physical and mechanical parameters of strata in Tashidian Erjingting Mine.

Lithology	Unit Weight (KN/m ³)	Compressive Strength (MPa)	Tensile Strength(MPa)	Elasticity Modulus (MPa)
Loose stratum	22	3.23	0.01	30
Sandy conglomerate	25.3	25.4	6.75	1400
Mudstone	24	28.4	3.56	1550
Siltstone	25.6	37.67	8.12	1450
Medium sandstone	23.6	20.4	5.02	1300

3. Materials and Methods

3.1. Physical Analog Model

Fully mechanized top coal caving of the whole seam is quite tricky, which would inevitably cause severe damage to the overlying strata and abnormal development of the water-conducting fracture zone [31,32]. Moreover, on account of the complex geological conditions of the research area, field tests showed a high cost and low feasibility. As a result, ideal observation conditions were difficult to obtain. By contrast, tests based on the established physical model can display the movement of overlying strata and the development of water-conducting fractures not only visually but also accurately predict the development height of the water-conducting fracture zone. Therefore, we established a physical model on similar materials to reveal the development characteristics of water-conducting fractures in weakly cemented overlying strata of the western Jurassic coal mine. We based it on a reasonable generalization of the geological mining conditions of the W8203 working face in Tashidian Erjingtian Coal Mine. Figure 4 shows the detailed model parameters.

5.3 cm		Soil zone
12.5 cm		Glutenite
28.9 cm	Aquiclude G1	Mudstone
32.3 cm	Aquifer H1	Glutenite
9.0 cm		Siltstone
18 cm		Medium sandstone
18 cm	Aquifer H2 (G2)	Siltstone
5.2 cm		Mudstone
9.0 cm		Siltstone
6.6 cm		Mudstone
13 cm	Aquifer H3	Siltstone
1.5 cm		Siltstone
1.5 cm		Siltstone

Figure 4. Illustration of the design of the present similar materials model test.

Three similarity theorems, namely, the positive similarity theorem (the first theorem), the π theorem (the second theorem), and the inverse similarity theorem (the third theorem), are the theoretical foundations for constructing a physical analog model. Our research test model used the test platform developed by Mine Pressure and Strata Control Laboratory, Xinjiang University, as shown in Figure 5, with a length \times width \times height of 250 cm \times 30 cm \times 190 cm. The depth of strata in this study is 499.02 m. Based on the specifications of the test devices and taking into full consideration the experimental condition, we overcame the challenges in construction and safety during the whole experimental process. The geometrical factor of the physical analog model was 1:300; the volumetric weight ratio and the dynamic ratio were 1:1.5 and 1:450.

Considering the weakly cemented properties of kaolin and the overlying strata in Tashidian Erjingtian Mine [33], this study selected river sand as the aggregates and kaolin and gypsum as the cementing materials for constructing the physical analog model test on the W8203 working face. We determined the mixing proportions and water mass ratios based on the related experimental results in the Similarity Theory and the Static Model Test [33]. We validated the reliability of the modeling ratios with the tests performed on the prepared samples (see Figure S1 in Supplementary Material). We added an appropriate gypsum retarder to the test materials to lower the material setting velocity. As shown in Figure 6a, we made three specimens from each stratum according to the proportion. Figure 6b shows the measurement of the uniaxial compressive strength test. The mean of the measured strengths validated the reliability of the ratios. According to the present measured data of uniaxial compressive strength, the selected proportions of similar proportioned materials satisfied the compressive strength criterion for the current similar model test. Table 3 lists the ratios for each stratum.

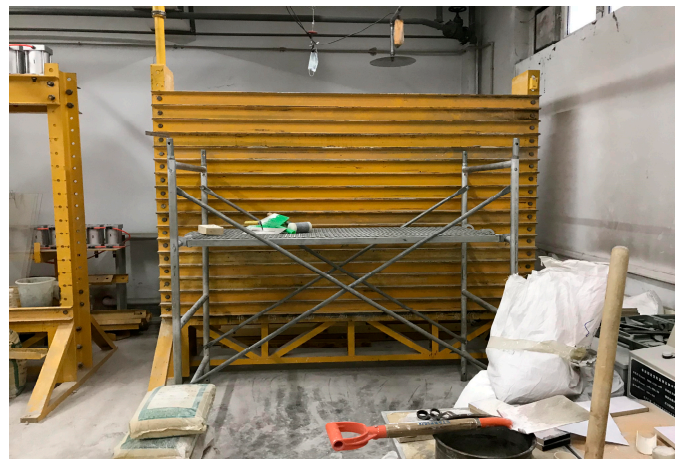


Figure 5. Test platform developed by the Mine Pressure and Stratum Control Laboratory.



(a)



(b)

Figure 6. Tests performed on the samples: (a) view of the test samples, a group of three test samples from left to right are siltstone, mudstone, medium sandstone and sandy conglomerate; (b) uniaxial compressive strength measurement on the prepared test samples.

Table 3. Proportions for preparing the materials similar to the overlying strata in Tashidian Erjingtian Mine.

Lithology	Unit Weight of Original Stratum (KN/m ³)	Compressive Strength of Original Stratum (MPa)	Unit Weight of the Model (KN/m ³)	Compressive Strength of the Model (kPa)	Proportion	Water Mass Ratio
Loose stratum	22	3.23	14.7	7.18	7:0.9:0.1 (791)	1/9
Glutenite	25.3	25.4	16.9	56.44	6:0.7:0.3 (673)	1/9
Mudstone	24	28.4	16	63.11	5:0.7:0.3 (573)	1/9
Siltstone	25.6	37.67	17.1	83.71	4:0.5:0.5 (455)	1/9
Medium sandstone	23.6	20.4	15.7	45.33	7:0.7:0.3 (773)	1/9

Before laying the physical analog model, the experimental platform was cleaned up, and lubricating oil was evenly applied on the inside of each guard plate to prevent damage to the physical analog model when the guard plate was disassembled. The gap was sealed with tape between the bottom guard plate and the model frame to prevent the leakage of test materials. Following the previous similar material, the ratio was determined, the use of electronic scales and measuring cylinders accurately measured experimental materials in the water to add an appropriate amount of gypsum retarder to delay the consolidation of the material progress, and an electric stirrer evenly stirred after laying. The laying model

was layered, and the compacted sleeper and hammer were used to push the compaction evenly. After the compression, the leveling, as combined with the level, the plastering knife was used to smooth, and the mica sheet was added between adjacent rock layers to achieve the stratification effect. After the physical analog model was cured under constant temperature and humidity for seven days, the board was dismantled. When the panel was dismantled, the single guard plate was dismantled on the front side of the model, and the even guard plate was disassembled on the back side. Then, the guard plate was dismantled alternately regularly until the guard plate was dismantled entirely.

We monitored the movements in the overlying strata and the evolution of water-conducting fractures in a similar physics model during the mining process (see Supplementary Material Figure S2 for the detailed laying process of the physical analog model). This study used pins and coordinate papers to set the grids with a size of 10 cm × 10 cm. We used a professional digital camera to record the whole experimental process before and after model excavation, as shown in Figure 7. Aiming to eliminate the boundary effect, we reserved 40 cm margins on two sides of the established similar physical model. The W8203 working face advanced at a speed of approximately 2.4 m/d. According to the time similarity constant, the model excavated forwards 10 cm every 17 h (actually, 30 m in 12.5 days), i.e., 17 excavations were required. In this study, we mined the coal seams from left to right.

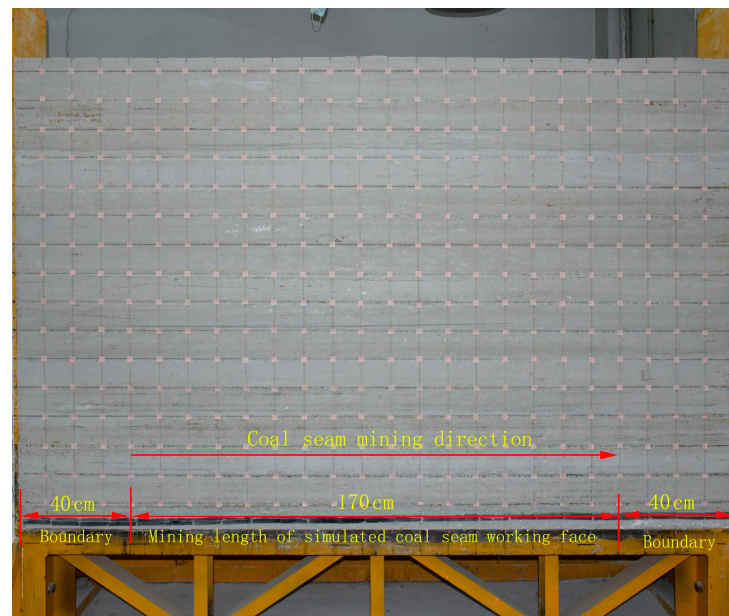


Figure 7. Established similar materials physical model.

3.2. Experimental Result

The mudstone false roof with a thickness of 3 m existed above the No. 8 coal seam in the W8203 working face. According to the experimental results, the water-conducting fractured zone began to develop with the forward advance. As the working face moved forward to 0–120 m, the height of the water-conducting fracture zone was maintained at 3 m, as shown in Figure 8a,b.

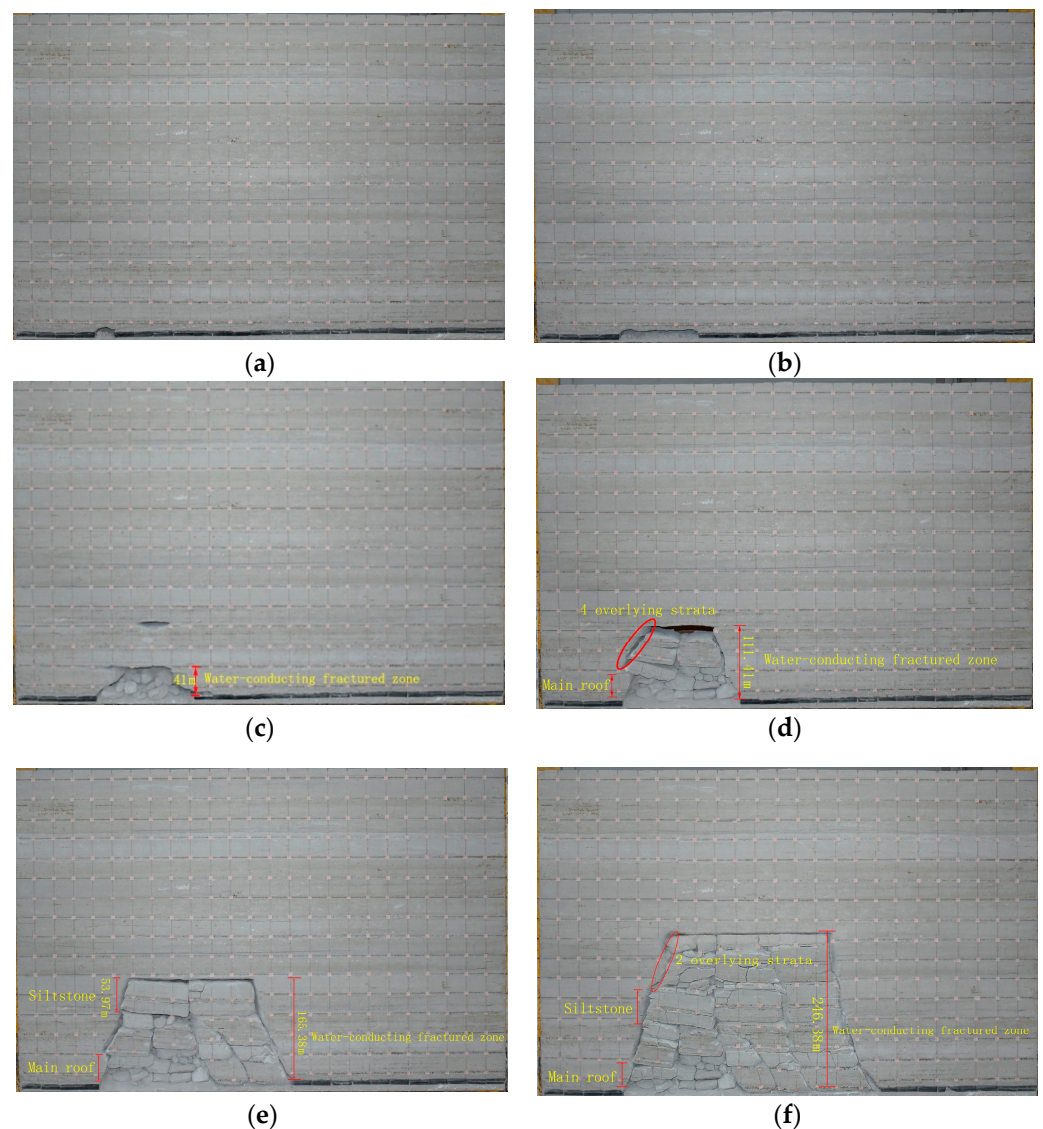


Figure 8. Overburden fracture characteristics: (a) rock mass failure as the working face moved forward to 30 m; (b) rock mass failure as the working face moved forward to 120 m; (c) rock mass failure as the working face moved forward to 150 m; (d) rock mass failure as the working face moved forward to 180 m; (e) rock mass failure as the working face moved forward to 300 m; (f) rock mass failure as the working face moved forward to 390 m.

As the working face gradually moved forward, the mudstone false roof collapsed, and the dangling distance below the main roof increased. As a result, the false roof fractured at an excavated length of 150 m, which drastically increased the caving zone's height. Concurrently, the water-conducting fractured zone's size changed abruptly to 41 m, as shown in Figure 8c. As the working face moved forward to 180 m, four overlying strata (mudstone, siltstone, medium sandstone, and mudstone strata) of the main roof fractured with the main roof. After the fracturing, the rocks formed a stable hinged structure. As a result, water-conducting fractures developed rapidly below the upper siltstone stratum with a thickness of 53.97 m, and the development height rapidly reached 111.41 m, as seen in Figure 8d.

As the working face moved forward, the main roof and the upper four overlying strata underwent periodic fractures. The development of the water-conducting fracture zone was stagnant, with an almost fixed height (approximately 111.41 m). As a result, the dangling distance below the siltstone stratum, with a thickness of 53.97 m, increased. As the work-

ing face moved to 300 m, the siltstone stratum underwent the first fracture, and the fractured rocks formed a stable hinged structure. The water-conducting fractures then rapidly developed above the siltstone stratum, and the development height increased rapidly to 165.38 m, as shown in Figure 8e.

As the working face further moved to 330 m, the two overlaying strata (medium-sandstone and siltstone strata) were fractured, accompanied by the fracturing of the lower siltstone stratum with a thickness of 53.97 m. The fractured rocks then formed a stable hinged structure, and the water-conducting fractures developed rapidly to below the ultra-thick gravel stratum with a thickness of 96.85 m, accompanied by the abrupt change in the development height to 246.38 m. As the working face moved forward to 390 m, the overlying strata underwent periodic fracturing, and the water-conducting fracture zone no longer developed upward. As shown in Figure 8f, the development height remained at 246.38 m.

As the working face moved to 510 m and mining was completed, we observed the gravel stratum with a thickness of 96.85 m after the overlying stratum was fully stable. No apparent fractures and cracks noticeably occurred in the gravel stratum. The water-conducting fracture zone stopped the development and maintained its height at 246.28 m—a significant “八”-shaped longitudinal fracture formed from the left side’s open-off cut extending to the right’s mining stop. As shown in Figure 9, the caving strata on the top of the goaf showed saddle-shaped distribution. According to the theory of the upper three zones, it developed the caved zone, the fractured zone, and the continuous deformation zone in the overlying strata of the W8203 working face. Based on the measured results in Tashidian Erjingtian Mine, the height of the water-conducting fracture zone on the roof of the No. 8 coal seam was 229.32 m. The measured value was close to the simulation data with the physical analog model, suggesting the reliability of the present physical analog model tests.

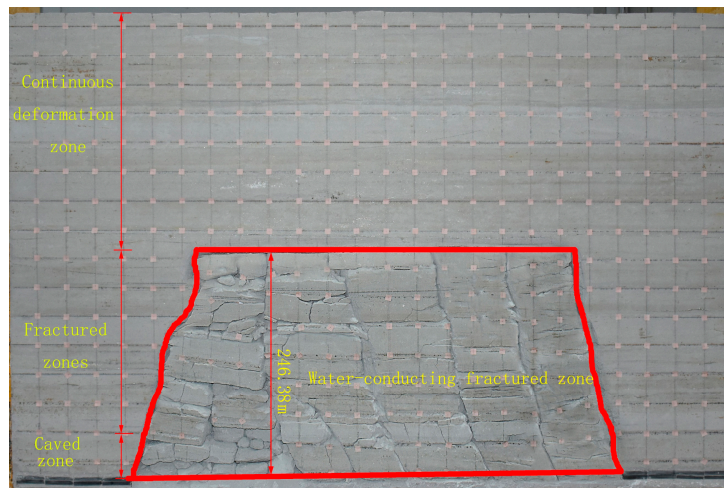


Figure 9. Rock mass failure as the working face moved forward to 510 m.

4. Theoretical Analysis of the Evolution Laws of Water-Conducting Fractures

4.1. Brief Introduction to Key Stratum Theory

Based on roof strata’s research and practice results for many years, academician Ming-gao Qian proposed the key stratum theory and the definitions of primary key stratum and sub-key stratum [34]. The primary key stratum was the stratum, which played a decisive role in the rock movement. In contrast, the sub-key stratum referred to the stratum, which played a decisive role partly in rock movements. The key strata in the overlying strata of the stope showed the following characteristics:

- (1) In terms of geometric characteristics, the key strata were thicker than the other strata.
- (2) Regarding lithological characteristics, key strata were more rigid than others.

- (3) In terms of deformation characteristics, the key strata sink in synchronized and coordinated patterns with the whole or part of the overlying strata.
- (4) In terms of fracture characteristics, the fracture of key strata can rupture the whole or part of the overlying strata.
- (5) In terms of bearing characteristics, the plate or beam structure of the stratum before the failure serves as the primary bearing structure of the whole or part of the strata, i.e., the key strata after fracture still show the bearing capacity to a certain degree.

4.2. Determination Method of the Locations of Key Stratum

We judged the locations of key stratum according to the following procedures.

First, we determined the locations of hard strata in the overlying strata based on the calculated loads. As described in [34], the load on the stratum included two parts—the load induced by the self-gravity and the load caused by the interaction of the upper strata (see Figure 10). The load on the stratum could be calculated using Equation (1). If the overlying load $q_{n+1} < q_n$, the n -th layer was a key stratum. All hard strata that satisfy the above conditions were the key strata.

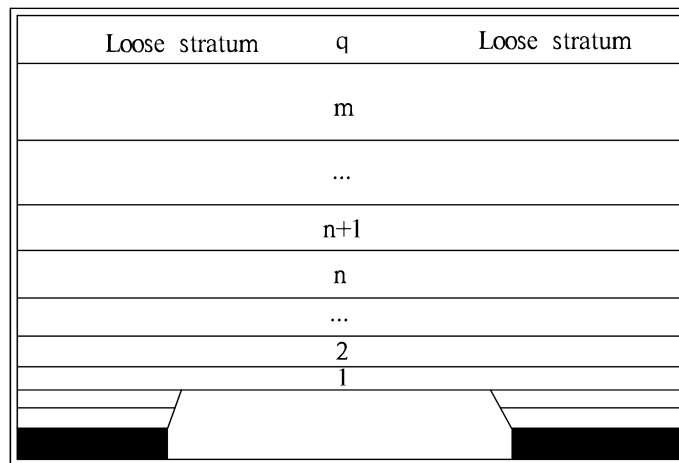


Figure 10. Calculation model of the load on the stratum [34].

We calculated the load on the stratum as:

$$(q_n)_1 = \frac{E_1 h_1^3 (r_1 h_1 + r_2 h_2 + \dots + r_n h_n)}{E_1 h_1^3 + E_2 h_2^3 + \dots + E_n h_n^3} \tag{1}$$

where E_1, E_2, \dots, E_n denote the elastic modulus of the 1st, the 2nd,... and the n th strata, respectively, with a unit of MPa; h_1, h_2, \dots, h_n denote the thicknesses of the 1st, the 2nd,... and the n th strata, respectively, with a unit of m; $\gamma_1, \gamma_2, \dots, \gamma_n$ denote the body forces on the 1st, the 2nd,... and the n th strata, respectively, with a unit of MN/m³.

Next, we took the judgment based on the calculated fracturing distances of various hard strata according to Equation (2). If the calculated fracturing distance $l_{n+1} > l_n$ was simultaneously satisfied, the hard stratum was the key stratum. Therefore, the fracturing distance was calculated as:

$$l = h \sqrt{\frac{2R_T}{q}} \tag{2}$$

where h was the thickness of the stratum, with a unit of m; R_T was the tensile strength of the stratum, with a unit of MPa; q was the load on the stratum, with a unit of MPa.

4.3. Determination of Key Strata in the Working Face

Based on the above-described judgment method of key strata, each stratum's load and fracturing distances were calculated layer by layer from bottom to top and compared with that of the adjacent strata to determine the location of the key stratum further.

Table 4 lists the overlying strata's physical and mechanical parameters in the W8203 working face. For the enhancement of calculation precision and the convenience of writing, the unit of the calculated load on the strata was converted into KPa.

Table 4. Physical and mechanical parameters of the overlying strata.

Serial Number of the Stratum	Lithology	Thickness of Stratum (m)	Body Force (MN/m ³)	Tensile Strength (MPa)	Elasticity Modulus (MPa)
1	Mudstone (false roof)	3.00	0.024	3.56	1550
2	Siltstone (main roof)	39.00	0.0256	8.12	1450
3	Mudstone	19.80	0.024	3.56	1550
4	Siltstone	27.00	0.0256	8.12	1450
5	Medium sandstone	6.92	0.0236	5.02	1300
6	Mudstone	15.69	0.024	3.56	1550
7	Siltstone	53.97	0.0256	8.12	1450
8	Medium sandstone	54.00	0.0236	5.02	1300
9	Siltstone	27.00	0.0256	8.12	1450
10	Glutenite	96.85	0.0253	6.75	1400
11	Mudstone	86.66	0.024	3.56	1550
12	Glutenite	37.63	0.0253	6.75	1400
13	Loose stratum	15.90	0.022	0.01	30

Based on the calculated results (see Equations (S1)–(S10) in Supplementary Material), the 1st stratum and the 2nd stratum were hard, and the fracturing distances of the mudstone false roof and the 2nd siltstone stratum satisfy the condition: $l_1 < l_2$. Therefore, both mudstone false roof and main roof were identified as key strata. Due to the limited space in this study, the calculation processes for many strata were tedious and not repeated here. However, through calculation, there existed four key strata in the overlying strata of the W8203 working face from bottom to top; namely, the 1st mudstone, the 2nd siltstone, the 7th siltstone, and the 10th glutenite strata, in which the 10th glutenite stratum was the primary key stratum and the rest were sub-key strata (see Table 5).

Table 5. Calculation results of key strata of working face W8203 of Tashidian Erjingtian Mine.

Key Stratum	Serial Number of Strata	Lithology	Load on the Stratum (KPa)	Fracturing Distance (m)
Sub-key stratum 1	1	Mudstone	75.900	29.056
Sub-key stratum 2	2	Siltstone	1749.111	118.836
Sub-key stratum 3	7	Siltstone	1654.379	169.094
Primary key stratum	10	Glutenite	3149.173	200.525

4.4. Application of Key Stratum Theory

Based on the similar model test results of the W8203 working face and the related monitoring data, the variation curves of the development height of the fractured water-conducting zone in the roof of the coal seam with the advancing distance were plotted, as shown in Figure 11.

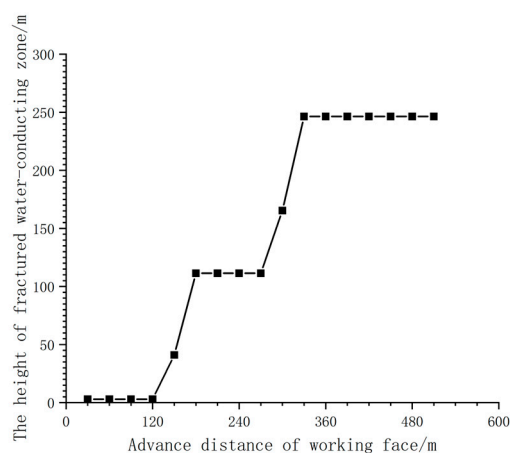


Figure 11. Statistics of the height of the water-conducting fracture zone with the physical analog model.

As shown in Figure 10, the height of the water-conducting fracture zone did not increase with the advancing distance in a simple linear pattern, attenuation, and mutation. Next, based on the physical analog model experimental result and key stratum theory, we dynamically analyzed the development process of water-conducting fractures in the W8203 working face.

Based on the judgment results of the locations of key strata in the working face, the mudstone false roof with a thickness of 3 m was determined as the sub-key stratum 1. The sub-key stratum 2 was above the sub-key stratum 1; therefore, the latter had no controlled stratum, which fell with mining during the advancing process. Therefore, a water-conducting fracture zone immediately developed when the W8203 working face began to move forward. At an advancing range of 0~120 m, the height of the water-conducting fracture zone was 3 m. As the operational front of the working face moved to 150 m, the sub-key strata 2 was first fractured, and the height of the water-conducting fracture zone changed abruptly and briefly stayed at 41 m. As the working face moved to 180 m, four strata controlled by the sub-key stratum underwent the first fracture, and the height of the water-conducting fracture zone developed upwards to the bottom of the sub-key stratum 3 and reached up to 111.41 m. Afterward, as the working face moved to 180~279 m since the sub-key stratum showed no fracturing, the development of water-conducting fractures was stagnant. As the working face moved to 300 m, the suspended span below the sub-key stratum 3 reached the limit of caving fracturing distance. At that moment, the sub-key stratum 3 was fractured first, and the height of the water-conducting fracture zone changed abruptly and briefly stayed at 165.38 m. As the working face moved to 330 m, two overlying strata controlled by the sub-key stratum 3 fractured first, the water-conducting fractured zone developed upwards, and the water-conducting fracture height changed abruptly to the bottom of the primary key stratum, reaching up to 246.38 m. As the working face moved from 330 to 510 m (the terminal mining line), the primary key strata were not fractured, and the development of water-conducting fractures tended to be stable and showed no change. Finally, the height of the water-conducting fracture zone was maintained at 246.38 m.

5. Discussion

By combining similar material physical model simulation, field monitoring, and theoretical analysis, this study explored the fracture characteristics of weakly cemented overlying strata and the evolution rules of water-conducting fractures. We found that the weakly cemented overlying strata in western China were easily deformed and fractured, and key strata controlled the development height of the water-conducting fracture zone on the roof. When the key or sub-key strata were not cracked, the height of the water-conducting frac-

tured zone stagnated in development. When the primary key or sub-key strata were fractured, the size of water-conducting fractures changed abruptly. According to the collected data, 28.57% of strata were regarded as mediocre hard strata, while 71.43% were soft and weak. Only a few key strata controlled the movement of strata in the weakly cemented overlying strata.

Additionally, most of the mechanical properties of the weakly cemented rocks in western China were smaller than the lower limits of the parameters in similar rocks of central and east China [22]. Accordingly, the key strata in the stopes of western China were more easily fractured than those in central and east China. The weakly cemented rocks in west China also have a smaller residual bulking coefficient than those in eastern and central China, thereby showing a consolidation phenomenon similar to the soil under sufficient pressure [35–37]. Atmospheric precipitation and snow melt water recharge groundwater through vertical infiltration of surface rock pores and fissures. Coal seam mining will produce water-conducting fractures, communicate the upper aquifer, and other recharge methods will flow into the goaf. Through the drainage system and the drainage of the goaf water, it will be discharged to the surface to ensure safe production. The weakly cemented strata quickly disintegrated when encountering water. Once the interconnected water-conducting fractures were formed, the water circulation would aggravate this phenomenon in addition, and the residual bulking coefficient can even be 1 [3]. Accordingly, under the same mining height, the variation of the caved zone in the western weakly cemented overlying strata was more evident than those in the overlying strata of central and east China when compacted and stabilized. Compared with the rocks of central and east China, it was not easy to form a stable hinged structure after the rock stratum was broken, leading to the greater height of water-conducting fractures in the western weakly cemented strata. Some previous studies proved the conclusion.

According to the statistics in [38], researchers found that the fracture-to-mining ratio of the deeply buried coal seam in Dongsheng Coal of western China ranged from 17.2 to 24. The statistics in [39] revealed that the fracture-to-mining ratio of the deeply buried coal seam in the Hujerte Mine in western China ranged from 17.7 to 24.56. Based on the statistics of the collected cases in [3], the fracture-to-mining ratio of nearly 50% of weakly cemented strata in large-mining-height working faces exceeded 15. Even seriously, the fracture-to-mining ratio of the S19 drill in the No. 31401 working face of the Qilianta Coal Mine reached 34.98. the fracture-to-mining ratio of No. 23101 working face in Buertai Coal Mine reached 48.67. The fracture-to-mining ratio can rarely be excellent in the Carboniferous-Permian large-mining-height working front. It was noted that the mining height of Tashidian Erjingtian Mine was 9.6 m, and the measured size of the water-conducting fracture zone was 229.32 m, with a fracture-to-mining ratio of 23.89, fitting well with the existing research results.

In this study, by collecting the measured data of the height of the water-conducting fracture zone in different mining areas and physical analog model, the characteristics that the weakly cemented overburden in the west was easy to deform and destroy and the height of the water-conducting fracture was higher than that of the similar stopes in the central and eastern mining areas were qualitatively demonstrated. Under the background that the development of mining areas in east and central China is approaching the end and the 'strategic westward shift' of coal resource exploration and development, this feature needs to be paid attention to by practitioners. In the future, various research methods will be used to strengthen the research on the development height of the water-conducting fracture zone of the weakly cemented overburden in the western Jurassic coal mine to provide a basis for green and safe production in mining of the west area. By collecting the measured height data of the fractured water-conducting zone of the Jurassic coal seam in western China, the prediction formula of the water-flowing fractured zone height of the Jurassic coal seam roof in western China is given by multiple regression analysis. The physical analog model, numerical simulation, theoretical analysis, and field measurement

are combined to study the fracture law of overburdened rock and the development height of the water-conducting fracture zone from multiple dimensions.

6. Conclusions

The present research results can provide theoretical support for safety products in the Tashidian Coal Mine and offer guidance for safety products in the western Jurassic coal mines. The main conclusions are outlined.

- (1) Using the established physical analog model, the fracturing characteristics of overlying strata in the W8203 working face and the evolution rules of the water-conducting fracture zone were investigated in depth. Experimental results revealed that the development height of water-conducting fractures on the roof of coal seam did not linearly increase with the advancing of the working face, certain stagnation, and mutability. Finally, the development height of the water-conducting fracture zone was 246.38 m.
- (2) Based on the upper-three-zone theory, the caved zone, the fractured zone, and the continuous deformation zone in the overlying strata of the W8203 working face all developed. According to the measured data, the height of the water-conducting fracture zone in the No. 8 coal seam was 229.32 m. The measured value is close to the test result, which can objectively confirm the experimental reliability.
- (3) Based on key-stratum theory, we determined that one primary key-stratum and three sub-key strata existed in the overlying strata of the W8203 working face of Tashidian Erjingtian Mine. The key strata controlled the development height of the water-conducting fracture zone. When the primary key stratum or sub-key stratum was fractured, the size of the water-conducting fracture zone developed abruptly.
- (4) Overall, the heights of water-conducting fractures in the weakly cemented overlying strata of western China exceeded that of similar stopes of central and east China. This should arouse great attention from the practitioners. Researchers should strengthen the research on the development height of the water-conducting fracture zone in the Jurassic weakly cemented overlying strata of western China to provide the basis for safety and green production in the western mines.

Supplementary Materials: The following supporting information can be downloaded at: <https://www.mdpi.com/article/10.3390/w15061097/s1>, Figure S1: Tests performed on the samples; Figure S2: Laying of physical analog model; Equations (S1)–(S10): Calculation process of key layer.

Author Contributions: Conceptualization, L.Z. (Lifei Zhang), Z.Z. and K.W.; investigation, L.Z. (Lifei Zhang), X.T., T.Z. and L.Z. (Lei Zhang); writing—original draft preparation, L.Z. (Lifei Zhang); writing—review and editing, Z.Z. All authors have read and agreed to the published version of the manuscript.

Funding: This research received no external funding.

Institutional Review Board Statement: Not applicable.

Informed Consent Statement: Not applicable.

Data Availability Statement: Not applicable.

Conflicts of Interest: The authors declare no conflict of interest.

References

1. Arnould, M. Discontinuity networks in mudstones: A geological approach. *Bull. Eng. Geol. Environ.* **2006**, *65*, 413–422. [[Cross-Ref](#)]
2. Bhattarai, P.; Marui, H.; Tiwari, B.; Watanabe, N.; Tuladhar, G.R. Influence of weathering on physical and mechanical properties of mudstone. *Phys. Rev. B* **2006**, *80*, 308–310.
3. Sun, L.H. Structural Evolution and Rock Pressure Activity Regularity of Weakly Cemented Strata of Large Mining Height Work Face in Western China. Ph.D. Thesis, University of Science and Technology Beijing, Beijing, China, 2017.

4. Brok, S.; Spiers, C.J. Experimental evidence for water weakening of quartzite by microcracking plus solution-precipitation creep. *J. Geol. Soc.* **1991**, *148*, 541–548. [[CrossRef](#)]
5. Erguler, Z.A.; Ulusay, R. Water-induced variations in mechanical properties of clay-bearing rocks. *Int. J. Rock Mech. Min.* **2009**, *46*, 355–370. [[CrossRef](#)]
6. Hadizadeh, J.; Law, R.D. Water-weakening of sandstone and quartzite deformed at various stress and strain rates. *Int. J. Rock Mech. Min.* **1991**, *28*, 431–439. [[CrossRef](#)]
7. Heggheim, T.; Madland, M.V.; Risnes, R.; Austad, T. A chemical induced enhanced weakening of chalk by seawater. *J. Pet. Sci. Eng.* **2005**, *46*, 171–184. [[CrossRef](#)]
8. Lajtai, E.Z.; Schmidtke, R.H.; Bielus, L.P. The effect of water on the time-dependent deformation and fracture of a granite. *Int. J. Rock Mech. Min.* **1987**, *24*, 247–255. [[CrossRef](#)]
9. Song, C.Y. The Analysis and Application of Mesoscopic Structure Characteristic and Deformation and Failure Mechanism of Weak Cemented Sandstone. Ph.D. Thesis, University of Science and Technology Beijing, Beijing, China, 2017.
10. Meng, Q.B. Study on Structure and Mechanical Properties and Constitutive Model of Very Weakly Cemented Rock. Ph.D. Thesis, China University of Mining and Technology, Xuzhou, China, 2014.
11. Akai, K.; Adachi, T.; Tabushi, N. Mechanical Properties of Soft Rock in Terms of Effective Stress. *J. Soc. Mater. Sci. Jpn.* **1974**, *23*, 368–373. [[CrossRef](#)]
12. Scott, T.E., Jr.; Abousleiman, Y.; Zaman, M. Acoustical imaging and mechanical properties of soft rock and marine sediments. *Off. Sci. Tech. Inf. Tech. Rep.* **2002**, *7*, 227–241.
13. Nakagawa, S.; Myer, L.R. Mechanical and acoustic properties of weakly cemented granular rocks. In Proceedings of the 38th U.S. Symposium on Rock Mechanics (USRMS), Washington, DC, USA, 7–10 July 2001.
14. Nong, X.; Towhata, I. Investigation of mechanical properties of soft rock due to laboratory reproduction of physical weathering process. *Soils Found.* **2017**, *57*, 267–276. [[CrossRef](#)]
15. Tommasi, P.; Verrucci, L.; Rotonda, T. Mechanical properties of a weak pyroclastic rock and their relationship with microstructure. *Can. Geotech. J.* **2015**, *52*, 1–13. [[CrossRef](#)]
16. Atapour, H.; Mortazavi, A. The influence of mean grain size on unconfined compressive strength of weakly consolidated reservoir sandstones. *J. Pet. Sci. Eng.* **2018**, *171*, 63–70. [[CrossRef](#)]
17. Komine, H. Simplified evaluation for swelling characteristics of bentonites. *Eng. Geol.* **2004**, *71*, 265–279. [[CrossRef](#)]
18. Li, L.M.; Larsen, I.; Holt, R.M. Laboratory Observation and Micromechanics-Based Modelling of Sandstone on Different Scales. *Rock Mech. Rock Eng.* **2015**, *48*, 1407–1422. [[CrossRef](#)]
19. Zhang, L.F. Study on Deformation and Failure Regular of Weak Cemented Overburden in Tashidian No.2 Coal Mine. Master's Thesis, Xinjiang University, Urumqi, China, 2021.
20. Nguyen, V.H.; Gland, N.; Dautriat, J. Compaction, permeability evolution and stress path effects in unconsolidated sand and weakly consolidated sandstone. *Int. J. Rock Mech. Min.* **2014**, *67*, 226–239. [[CrossRef](#)]
21. Xu, J.L. Research and progress of coal mine green mining in 20 years. *Coal Sci. Technol.* **2020**, *48*, 1–15.
22. Sun, L.H.; Ji, H.G.; Yang, B.S. Physical and mechanical characteristic of rocks with weakly cemented strata in Western representative mining area. *J. China Coal Soc.* **2019**, *44*, 866–874.
23. Islam, M.R.; Hayashi, D.; Kamruzzaman, A. Finite element modeling of stress distributions and problems for multi-slice longwall mining in Bangladesh, with special reference to the Barapukuria coal mine. *Int. J. Coal Geol.* **2009**, *78*, 91–109. [[CrossRef](#)]
24. O'Connor, K.M.; Dowding, C.H. Distinct element modeling and analysis of mining-induced subsidence. *Rock Mech. Rock Eng.* **1992**, *25*, 1–24. [[CrossRef](#)]
25. Palchik, V. Influence of physical characteristics of weak rock mass on height of caved zone over abandoned subsurface coal mines. *Environ. Geol.* **2002**, *42*, 92–101. [[CrossRef](#)]
26. Vyazmensky, A.; Elmo, D.; Stead, D. Role of Rock Mass Fabric and Faulting in the Development of Block Caving Induced Surface Subsidence. *Rock Mech. Rock Eng.* **2010**, *43*, 533–556. [[CrossRef](#)]
27. Wang, Z.S. Study on height of water-conducting fissure zone in working face of shallow thick coal seam. *Coal Eng.* **2021**, *53*, 66–70.
28. Young, M.; Walton, G.; Holley, E. Investigation of factors influencing roof stability at a Western U.S. longwall coal mine. *Int. J. Min. Sci. Technol.* **2019**, *29*, 130–134. [[CrossRef](#)]
29. Zechner, E.; Konz, M.; Younes, A.; Huggenberger, P. Effects of tectonic structures, salt solution mining, and density-driven groundwater hydraulics on evaporite dissolution (Switzerland). *Hydrogeol. J.* **2011**, *19*, 1323–1334.
30. Mashinskii, E.I. Elastic-microplastic nature of wave propagation in the weakly consolidated rock. *J. Appl. Geophys.* **2014**, *101*, 11–19. [[CrossRef](#)]
31. Teng, Y.H. Development features and max height calculation of water conducted fractured zone caused by fully mechanized top coal caving mining. *Coal Sci. Technol.* **2011**, *39*, 118–120.
32. Sellers, E.J.; Klerck, P. Modelling of the effect of discontinuities on the extent of the fracture zone surrounding deep tunnels. *Tunn. Undergr. Space Technol.* **2000**, *15*, 463–469. [[CrossRef](#)]
33. Yuan, W.Z. *Theory of Similarity and Statics Model Test*, 1st ed.; Press of Southwest Jiaotong University: Chengdu, China, 1998; pp. 1–59.

34. Qian, M.G.; Shi, P.W.; Xu, J.L. *Mining Pressure and Strata Control*, 2nd ed.; China University of Mining and Technology Press: Xuzhou, China, 2010; pp. 64–186.
35. Davis, E.H.; Raymond, G.P. A Non-Linear Theory of Consolidation. *Geotechnique* **1965**, *15*, 161–173. [[CrossRef](#)]
36. Gibson, R.E.; England, G.L.; Hussey, M.J.L. The theory of one-dimensional consolidation of saturated clays. *Geotechnique* **1967**, *17*, 261–273.
37. Lekha, K.R.; Krishnaswamy, N.R.; Basak, P. Consolidation of Clays for Variable Permeability and Compressibility. *J. Geotech. Geoenviron. Eng.* **2003**, *129*, 1001–1009.
38. Ju, J.F.; Ma, X.D.; Zhao, F.Q.; Liu, Y.J.; Wang, Y.Z.; Liu, L.; Xu, J.L. Evelopment and zoning characteristics of water—Conducted fractures in Dongsheng Coalfield. *Coal Sci. Technol.* **2022**, *50*, 202–212.
39. Yin, H.J. Study of Mechanism of Surface Subsidence When Deep Mining under the Weakly Cemented Overburden. Master's Thesis, China University of Mining and Technology, Xuzhou, China, 2020.

Disclaimer/Publisher's Note: The statements, opinions and data contained in all publications are solely those of the individual author(s) and contributor(s) and not of MDPI and/or the editor(s). MDPI and/or the editor(s) disclaim responsibility for any injury to people or property resulting from any ideas, methods, instructions or products referred to in the content.